🔓 OPEN ACCESS

The olfactory bulb endocast as a proxy for mammalian olfaction

Quentin Martinez[a,1] (ID), Cécile Molinier[b] (ID), Ilse K. Barraza-Soltero[a] (ID), Elena Berger[a], Kévin Le Verger[c] (ID), Anne-Claire Fabre[d,e,f] (ID), Guillaume Billet[g] (ID), Vincent Fernandez[f,h], Gabriel S. Ferreira[i,j] (ID), Thomas van de Kamp[k,l] (ID), Elias Hamann[k] (ID), Marcus Zuber[k] (ID), Roberto Portela Miguez[f] (ID), Lionel Hautier[f,m] (ID), and Eli Amson[a] (ID)

Affiliations are included on p. 10.

Olfaction is a critical sense for tetrapods, playing a key role in survival and reproduction by aiding in food detection, predator avoidance, and social interactions. Olfactory performance has been experimentally tested in only a few taxa, so comparative analyses rely on anatomical and genomic proxies. Among anatomical proxies, the olfactory bulb endocast is widely used, particularly in extinct species, where it is often the only preserved proxy and can be reconstructed even in million-year-old fossils. While the functional significance of chemoreceptor genes has received attention, the extent to which the olfactory bulb endocast correlates with genomic proxies remains unclear. Using brain endocasts across all mammalian orders, we investigated the relationship between the absolute (absOB) and relative (relatOB) volumes of the olfactory bulb endocast and the number of intact chemoreceptor genes. While no clear correlations were found between absOB and the genomic proxies tested, we identified a significant correlation between relatOB and the total number of combined intact chemoreceptor genes (CombChemo), primarily driven by olfactory receptor genes (OR). Leveraging this correlation, and aiming to infer olfactory capabilities in taxa for which only the skull is available, we estimated OR numbers for three mammalian orders lacking genomic data, as well as for five extinct mammals. Building on studies that have established a link between intact OR and olfactory sensitivity and discrimination, we conclude that relatOB enables inference of olfactory capabilities in mammals. This provides a basis to investigate sensory evolution and opens perspectives for interpreting paleoecology and behavior of extinct mammals.

paleontology | chemosensory | brain endocast | genomics | olfactory receptor genes

Olfaction is a critical sense for tetrapods, playing a fundamental role in their fitness by aiding in food detection, predator avoidance, and social interactions like mating. In mammals, the significance of olfaction is reflected in their genomes, where a substantial proportion of coding genes are dedicated to olfactory receptors (OR) (1–5). The increasing availability of high-quality genomic data has greatly enhanced our understanding of mammalian olfaction, revealing intricate links between species ecology and behaviors and this vital sensory system (6–12). However, despite these advancements in genomics, morphology remains indispensable, particularly for studying olfaction in extinct species, as genomic data cannot be recovered from old fossils. Morphological analysis provides the only means to trace the evolutionary trajectory of olfactory capabilities in deep time.

Several bony anatomical proxies have been employed to estimate olfactory capabilities in both extant and extinct species. These include bony structures such as the olfactory turbinals (10, 13–21) and the cribriform plate (22–24). While these proxies offer valuable insights, their often incomplete preservation in the fossil record restricts their incorporation into quantitative frameworks (25–27). In contrast, the olfactory bulb, as reconstructed from brain endocasts, has been reported to be well-preserved in thousands of fossils (28–37). Consequently, the olfactory bulb endocast has been extensively described and, in some cases, utilized in quantitative analyses (30, 37). With the advent of imaging technologies such as desktop- and synchrotron-based X-ray micro-computed tomography (micro-CT), the detailed examination of fossilized skulls has become more accessible. These technologies have sparked increased interest in the quantitative study of olfactory bulb endocasts. However, no comprehensive studies have yet tested the functional significance of the olfactory bulb endocast in mammals, particularly in relation to genomic proxies of olfaction. The central role of the olfactory bulb in processing olfactory information underscores its relevance as a morphological proxy. Odorant molecules enter the nasal cavity and bind to OR located in the olfactory epithelium. These receptors are linked to the olfactory bulb via axonal projections of olfactory sensory neurons, where the chemical signal is transmitted and integrated. As the primary brain structure receiving direct

Significance

Understanding how olfactory capabilities evolve is challenging, especially in extinct species where direct assessment of behavior is not possible. In mammals, the volume of the braincase reflects the volume of the brain. This study demonstrates that the relative volume of its anterior part, the olfactory bulb endocast, significantly correlates with the number of intact chemoreceptor genes, a genomic marker of olfactory function. Since the braincase is a bony structure often preserved in fossils, this finding validates the use of the olfactory bulb endocast as a proxy for estimating olfaction in extinct mammals. By bridging anatomy and genomics, these results provide a powerful tool to investigate sensory evolution and reconstruct behavioral ecology in deep time.

input from OR, the olfactory bulb centralizes the initial neural processing of odor cues, making it a key structure in assessing olfactory capabilities (7).

In this study, we aim to address existing knowledge gaps between phenotype and genotype by analyzing newly generated brain endocasts from 66 extant mammalian species spanning all orders. Specifically, we examined the relationship between the absolute (absOB) and relative (relatOB) volumes of the olfactory bulb endocast and the number of various intact chemoreceptor genes, including intact OR, vomeronasal receptor (VR), trace amine-associated receptor (TAAR), and taste receptor (TR) genes. Additionally, we investigated two combined genomic variables: the total number of intact olfactory receptor genes (CombOR; including OR, VR, and TAAR), which are associated with the sense of smell in a broad sense, and the total number of intact chemoreceptor genes (CombChemo; including CombOR and TR), which also incorporates the sense of taste (gustation), a modality hypothesized to be closely associated with olfaction (38).

Given the substantial variation in body mass across all mammals, we do not expect absOB to significantly correlate with the genomic proxies because of the size-related bias. However, we predict that relatOB should exhibit significant correlations with CombChemo, CombOR, and OR, while no significant correlations should be found with the other gene families. Such findings would provide strong evidence for the functional relevance of olfactory bulb endocasts in determining olfactory capabilities and open broad avenues for the understanding of the evolution of mammalian olfaction diversity in deep time.

1. Material and Methods

1.1. Brain Endocast Data Acquisition. For this study, 40 high-resolution micro-CT scans of undamaged skulls or ethanol-preserved heads, including at least one species per order, were obtained, while 31 were downloaded from MorphoSource (Dataset S1; 39). For the 40 new CT datasets, specimens were imaged using the Nikon Metrology HMX ST 225, Nikon XT H 320, RX EasyTom 150, Phoenix V tome x C450 Baker Hughes, Zeiss metrotom 1500 G3, and a noncommercial microtomograph built in-house at the Karlsruhe Institute of Technology (KIT). Image acquisition parameters and filter use varied among specimens to maximize image clarity and material penetration (Dataset S1).

The brain endocast of the 71 species was presegmented in Avizo 3D 2021.2 (Thermo Fisher Scientific), and interpolation was performed with Biomedisa (40). The interpolated result was then reimported into Avizo, individually checked, and the olfactory bulb endocast was manually refined. For the anterior delimitation of the brain endocast, the olfactory nerve casts were similarly cut with the lasso tool in Avizo, using the 3D virtual model of the brain endocast. This cut generally corresponds to the area just before the foramina open to the nasal cavity and the olfactory turbinals. The delimitation between the overall brain endocast and the olfactory bulb endocast was performed using the lasso tool in Avizo on the 3D virtual model. The olfactory bulb endocast includes both the main and accessory olfactory bulb. Generally, a distinct demarcation, referred to as the circular or annular fissure (28, 41), typically separates the olfactory bulb from the cerebrum. This fissure is generally well-defined, allowing a consistent separation of the olfactory bulb with careful observation. However, across mammals, we observed notable variation in this transitional zone. In some species, this area is broader, making the boundary between the olfactory bulb and the cerebrum less distinct. In such cases, we defined the anterior limit of the transitional area as the boundary of the olfactory bulb endocast. In species with a highly reduced olfactory bulb, such as sirenians (Figs. 1–4; 34, 42), or in proboscideans, where the olfactory bulb is less clearly differentiated (Figs. 1–4; 31, 43, 44), delimiting the olfactory bulb is more challenging. In such cases, operator consistency was crucial. Moreover, in some species, like humans or some mysticetes (45), the morphology of the olfactory bulb does not allow for the generation of a distinct olfactory bulb endocast. As highlighted with other olfactory proxies, where anatomical delineations can vary between operators, combining data from different research teams in fine-scale

quantitative studies may introduce unwanted variability (18). To limit potential confounding effects related to operator segmentation or chosen methodology, all brain endocasts were checked and cleaned, as well as delineated, by the same operator. The volumes of the olfactory bulb endocast, along with the measurement of the occipital condyle width (maximum width of both condyles), were extracted and measured using Avizo. The latter was used as a body size proxy following Engelman (46).

To include the olfactory bulb endocast of an adult mysticete in our dataset, we used a parasagittally sawed skull that preserves more than one lateral half of the brain endocast. This sawed skull was cataloged in the museum collection as *Megaptera novaeangliae* according to Georg Pilleri's attribution. However, the sawed skull elements do not match the surface scan of a complete *Megaptera* skull, but instead correspond to *Eubalaena* (*SI Appendix*, Method S1 and Fig. S1 and Dataset S2). This specimen included anteriorly more than half of the cribriform plate and posteriorly one occipital condyle. To confirm that the individual was an adult, the braincase was duplicated and mirrored in Blender, and the occipital condyle width was measured. The complete olfactory bulb endocast (including the olfactory tract) was segmented and separated from its olfactory tract by the same operators using the same methodology as for *Protocetus* (Fig. 5; 48), and the volume was doubled to represent, as in other mammalian samples, both bulbs. Since cetacean olfaction is still a field under active investigation, and olfactory bulb delimitation could be subject to debate, various analyses were replicated including or excluding cetaceans (see *Material and Methods* below).

A subsample of the original dataset was created by selecting one species per mammalian order to consider the potential bias of sampling the phylogenetic diversity of mammals nonuniformly. To test which body size proxy best fits our data, we used these 29 species (Dataset S1) and measured the volume of the olfactory bulb endocast and the maximum width of the occipital condyle, as well as the volume of the overall brain endocast. Particular attention was given to cleaning and refining the overall brain endocast segmentation in a standardized way across species. For the posterior delimitation, the brain endocast was digitally extended beyond the occipital condyle. Using the skull sagittal section from the 2D orthoslices, a line was then drawn between the most dorsoposterior and ventroposterior points of the occipital condyle across all images in the stack and the exterior elements of the brain endocast were removed. Subsequently, this posterior delimitation was refined in the 3D virtual model as follows: The 3D virtual skull surface was placed in ventral view, and the most ventroposterior point of the occipital condyle was aligned with its most dorsoposterior point. Once aligned, the inner part of the occipital condyle was drawn with the lasso tool and removed from the brain endocast. All brain endocasts were subsequently cleaned using the lasso tool on the 3D virtual model. For example, casts of various nerves (e.g., optic nerve), veins, and sphenorbital fissures were removed (see, for example, ref. 41). This step was carefully performed to avoid removing other parts of the brain endocast. With the subsampled dataset, the delimitation between the overall brain endocast and the olfactory bulb endocast was repeated three times for each endocast, and the mean of their volume was used in the subsequent statistical analyses. For genera with a reduced olfactory bulb (*Macaca* and *Trichechus*), where variation in olfactory bulb isolation may introduce significant quantitative differences, and for *Loxodonta*, where precise delimitation of the olfactory bulb is less evident than in the other studied genera, this process was repeated five times. Body size was also included in the analyses using the species body mass, obtained from the database of Smith et al. (49). For *Galeopterus variegatus* and *Macaca nemestrina*, the body mass of mainland individuals was selected. For *Tachyglossus aculeatus*, the body mass of individuals from Australia was chosen. Finally, the mass of *Galegeeska rufescens* was selected because it corresponds to the species chosen for the brain endocast, although it is not the same species for the genomic proxies (see below). Since several studies use brain mass as a metric, we also converted the brain endocast volume to grams by multiplying it by the brain tissue density (1.036 g/cm^3), following Stephan (50).

1.2. Genomic Data Acquisition. In this study, we aimed to use a genomic proxy of olfaction that is as close as possible to a functional proxy. Our aim was to estimate olfactory capabilities across species (51), rather than to investigate the evolutionary dynamics of olfactory gene families such as pseudogenization or gene duplication events. Although, in recent years, methodologies for determining the completeness of chemoreceptor genes have become quite similar, whether one should refer to these genes as "functional" or "intact" is still under
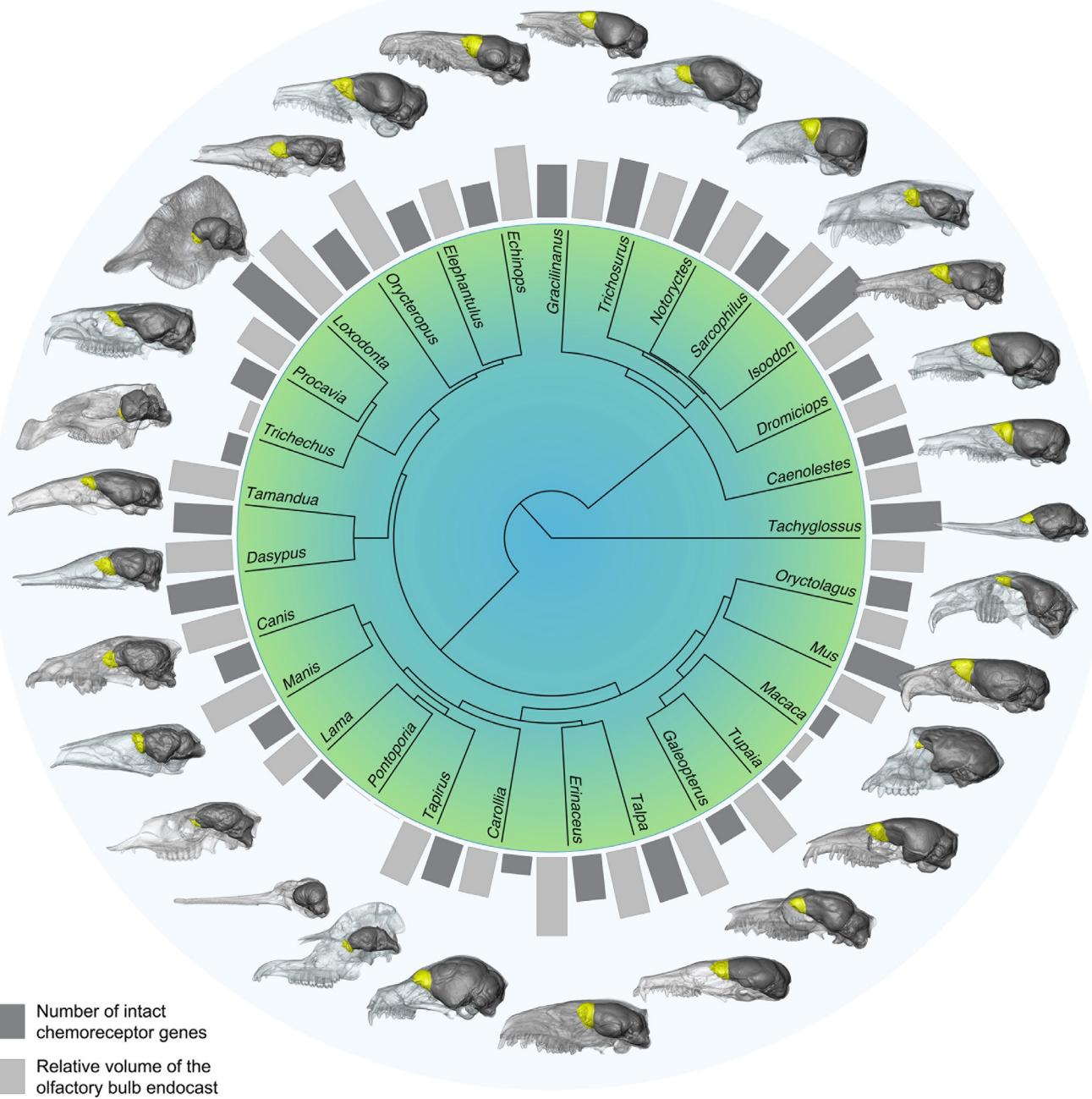
Fig. 1. Genomic and morphological olfactory disparity across all mammalian orders. Sagittal views of the skull and segmented brain endocasts are shown for the 29 orders of mammals. The olfactory bulb endocast is highlighted in yellow, and the rest of the brain endocast is depicted in dark gray. Barplots illustrate the relative volume of the olfactory bulb endocast (light gray) and the number of intact chemoreceptor genes (dark gray) derived from high-quality genomes. The relative volume of the olfactory bulb endocast is represented by the residuals of a linear regression between olfactory bulb volume and occipital condyle width (used as size proxy). Both the relative volume of the olfactory bulb endocast and the number of intact chemoreceptor genes were normalized for visualization (to a 0 to 1 range). The so-called "intact" genes in this study are also referred to as "functional" elsewhere (see *Material and Methods* for discussion). Tree topology is based on Upham et al. (47). Skulls are not to scale.

debate. This stems from the rapidly evolving nature of chemosensory gene families (52), as well as from cases in which fully aquatic amniotes, species thought to have limited reliance on olfaction, still retain some genes considered "intact" or "functional" (12, 53). The term "functional" appears to be the most widespread (8, 11, 12, 17, 18, 23, 54), compared to the term "intact" (52, 53, 55), although some teams use both terms or have changed their terminology over time (56). To be as conservative as possible, we use the term "intact" in this study but recognize that both terms refer to the same genes.

We extracted the numbers of intact OR genes, intact trace amine-associated receptors (TAAR) genes, intact vomeronasal receptor genes types 1 and 2 (V1R and V2R), and intact taste receptor genes types 1 and 2 (T1R and T2R) from Policarpo

et al. (12), using their category labeled "number.Complete7tm_X_Total". This category represents a conservative approach, as it includes only genes encoding a complete seven-transmembrane (7TM) domain. To provide a less restrictive comparison, we also used their category labeled "number.Complete_X_Total" and duplicated all analyses accordingly. The total number of intact vomeronasal receptor (VR) genes was calculated by summing V1R and V2R. The total number of intact taste receptor (TR) genes was calculated by summing T1R and T2R. The total number of combined intact olfactory receptor (CombOR) genes was obtained by summing OR, V1R, V2R, and TAAR. The total number of combined intact chemoreceptor (CombChemo) genes was obtained by summing OR, V1R, V2R, TAAR, T1R, and T2R. To provide results comparable to those of Policarpo et al. (12),
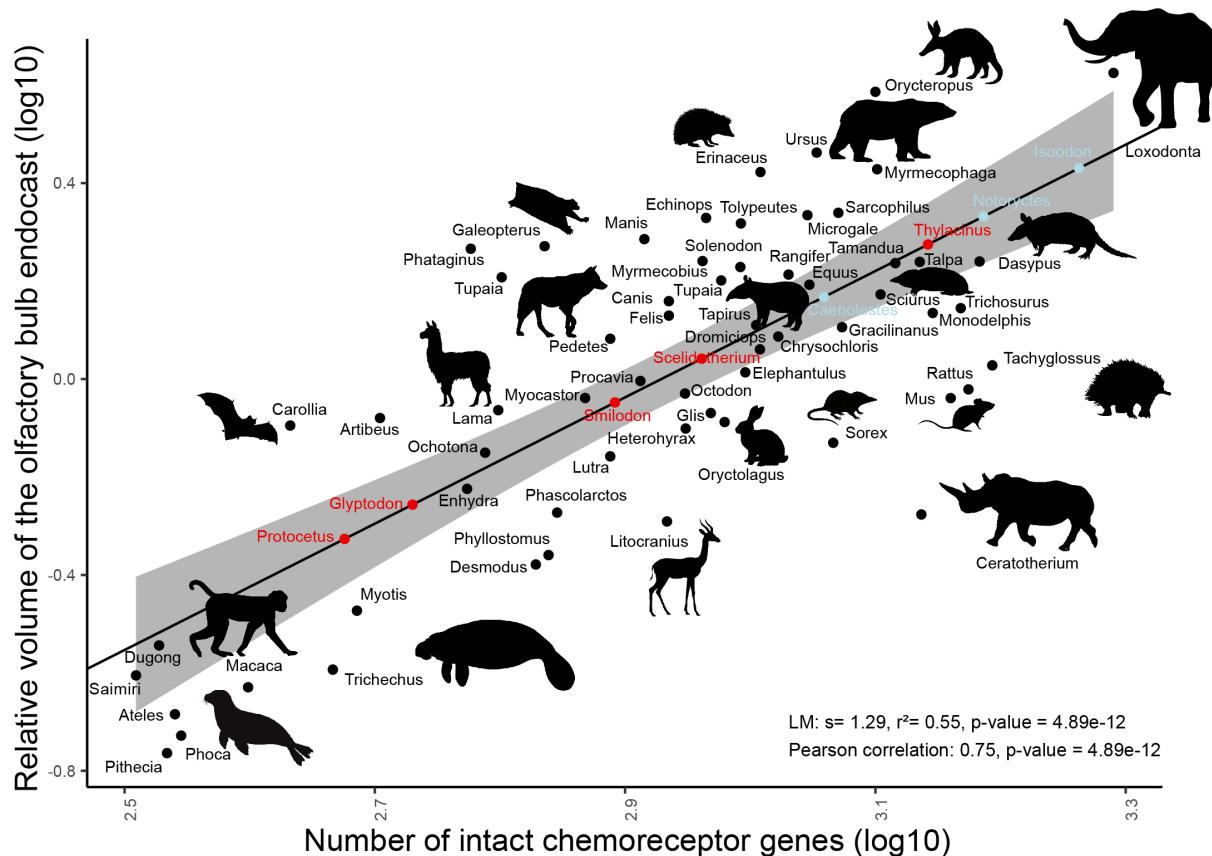
Fig. 2. The relative volume of the olfactory bulb endocast reflects the number of intact chemoreceptor genes. Significant regression (best fit was the ordinary linear model, LM; all tested PGLS models had either significantly worse fit or, for models that estimate most likely parameters, found values for those parameters entailing for the models to be the same as LM) between the relative volume of the olfactory bulb endocast (log10) and the number of intact chemoreceptor genes (log10) across 64 extant mammalian species and five emblematic extinct species. Red dots represent the five extinct species, for which gene counts were predicted. Light blue dots represent the three species (*Caenolestes caniventer*, *Isoodon macrourus*, and *Notoryctes typhlops*), for which gene counts were also predicted based on the linear regression. The so-called "intact" genes in this study are also referred to as "functional" elsewhere (see *Material and Methods* for discussion). Creative Commons silhouettes were obtained from https://www.phylopic.org or generated by DALL·E 3. In compliance with PhyloPic guidelines, we credited Gabriela Palomo-Muñoz, Roberto Díaz Sibaja, and Sarah Werning for the unmodified silhouettes of *Dasypus*, *Desmodus*, and *Loxodonta*, respectively, and provided the license link: https://creativecommons.org/licenses/by/3.0/.

the total number of intact TAAR genes was included in CombOR and CombChemo. However, it is important to note that TAAR1 is not selectively expressed in the olfactory epithelium (57). Additionally, to provide a comparison with a third methodology for extracting intact OR genes, developed by a different team, we gathered the OR data from the Chordata Olfactory Receptor Database (CORD; 53). For the genomic data, based on the available data, *Galegeeska rufescens* was replaced by *Elephantulus edwardii*, *Equus grevyi* by *Equus quagga*, *Artibeus lituratus* by *Artibeus jamaicensis*, *Saimiri sciureus*, by *Saimiri boliviensis* and *Talpa aquitania* by *Talpa occidentalis*. For *Canis lupus*, *Lama glama*, *Mus musculus*, *Enhydra lutris*, *Rangifer tarandus*, *Ceratotherium simum*, *Solenodon paradoxus*, and *Orycteropus afer*, two to four genomes were available, either due to the presence of different subspecies or multiple genome versions. In these cases, we selected the subspecies corresponding to the brain endocast data or chose the genome with the highest N50, representing the median contig or scaffold length for genome assembly quality.

1.3. Phylogeny and Statistics. We used a maximum clade credibility (MCC) phylogeny derived from 10,000 trees sampled from the posterior distribution of Upham et al. (47), pruned to include the 66 extant species in our dataset. For this phylogeny, *Talpa occidentalis* was used, whereas *Talpa aquitania* was used for the brain endocast data.

In the following analyses, *Pontoporia* was considered an outlier, as its inclusion or exclusion alters the normality and/or heteroscedasticity of various tests (see below). Therefore, for the following statistical tests, analyses were conducted using the dataset excluding *Pontoporia*. However, we also performed all subsequent analyses including *Pontoporia* to demonstrate that its inclusion or exclusion

does not affect the overall trends and conclusions of this study. For the analyses including *Pontoporia*, no olfactory bulb was identified; however, a value of 0.001 mm³ was arbitrarily assigned to this species to enable its inclusion in the quantitative analyses.

Based on the subsample composed of one species per mammalian order, we needed to determine the best size proxy to use in subsequent analyses for obtaining the relative volume or mass of the olfactory bulb. To do this, we performed an ordinary least squares regression (LM) between the absolute volume or mass of the olfactory bulb and various size proxies: body mass, total brain volume, and occipital condyle width. We then tested the normality of the residuals using the Shapiro–Wilk test. Since none met the validity conditions, we performed model comparisons using log10 transformations on both variables. Although normality was not achieved after transformation, the distribution improved (Shapiro–Wilk p-values, which should be >0.05, ranged from 4.00E−03 to 2.40E−02; Dataset S11). We then used the transformed data to test for significant correlations between absolute olfactory bulb mass and volume, and the different size proxies using Kendall and Spearman tests (Dataset S11). Since all correlation tests were significant, we proceeded with model comparisons based on the Akaike Information Criterion (AIC) to identify the best variable for data correction (Dataset S11). For each tested combination, we conducted ordinary least squares regression (LM), generalized least squares (GLS) without phylogeny, and phylogenetic generalized least squares (PGLS) using Martin, Grafen, and Brownian models. In general, LM using occipital condyle width or body mass provided the best model fits. Since occipital condyle width was measured on the same individual from which the olfactory bulb endocast was extracted, whereas body mass was obtained at the species level from different databases, we considered
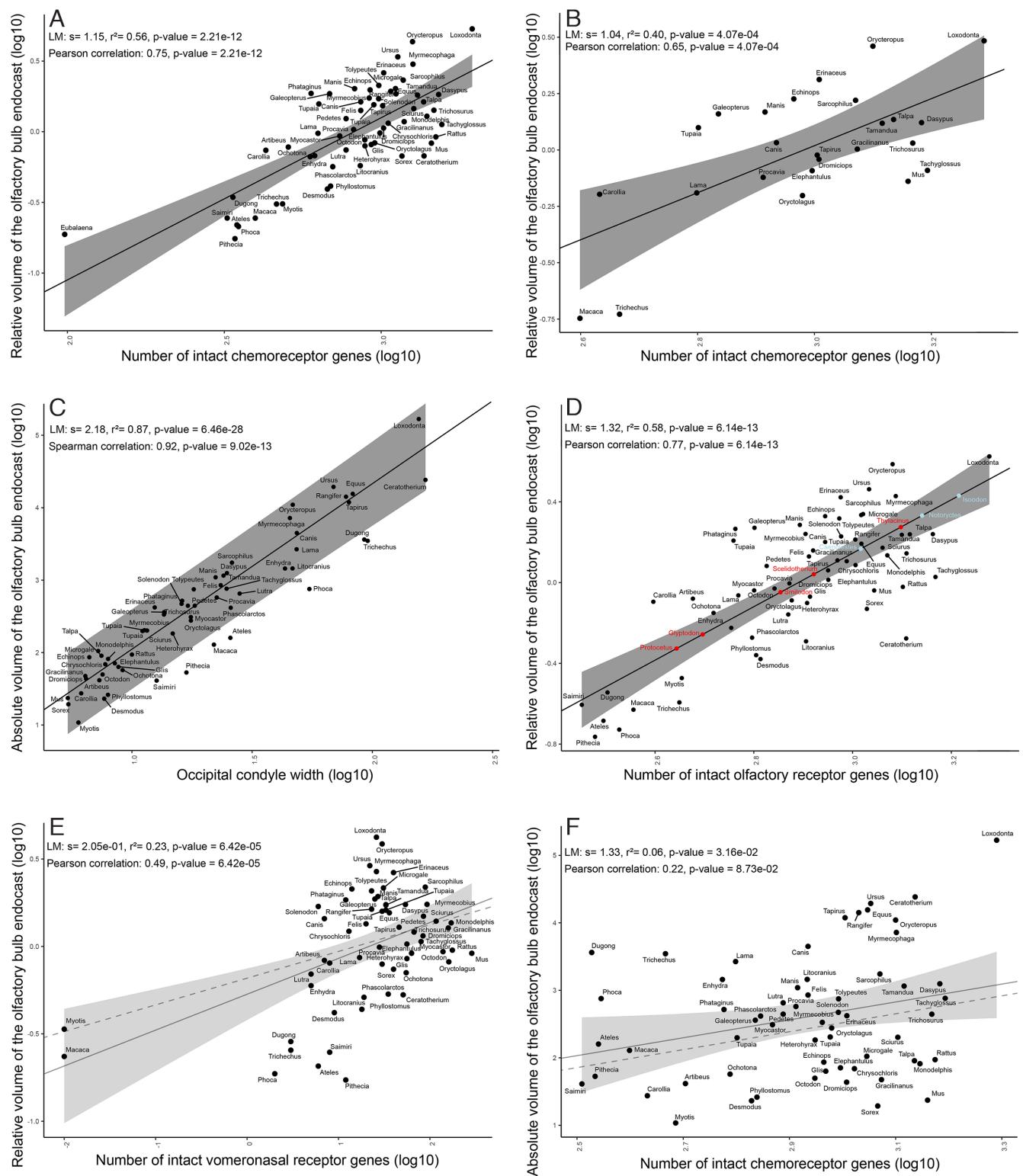
Fig. 3. Linear regressions (solid lines) and phylogenetic generalized least squares (dashed lines) illustrating genome-to-morphology correlations across extant and extinct mammalian species. (*A*) Relationship between the relative volume of the olfactory bulb endocast (log10) and the number of intact chemoreceptor genes (log10) based on the dataset including the right whale (*Eubalaena sp.*). (*B*) Relationship between the relative volume of the olfactory bulb endocast (log10) and the number of intact chemoreceptor genes (log10) based on the dataset including one species per mammalian order and excluding the cetaceans. (*C*) Relationship between the absolute volume of the olfactory bulb endocast (log10) and occipital condyle width (log10). (*D*) Relationship between the relative volume of the olfactory bulb endocast (log10) and the number of intact olfactory receptor (OR) genes (log10). (*E*) Relationship between the relative volume of the olfactory bulb endocast (log10) and the number of intact vomeronasal receptor genes (log10). The light gray color of the regression lines and CI indicates that, although the correlation is significant, we do not consider it reliable due to its low R-squared value, as well as because it is driven by outliers, particularly *Macaca* and *Myotis* (Table 1). (*F*) Relationship between the absolute volume of the olfactory bulb endocast (log10) and the number of intact chemoreceptor genes (log10). Although significant, we do not consider the latter two correlations (light gray color of the regression lines and CI) to be robust due to low R^2 value. A solid line alone indicates that the best-fit model was the LM. The so-called "intact" genes in this study are also referred to as "functional" elsewhere (see *Material and Methods* for discussion).
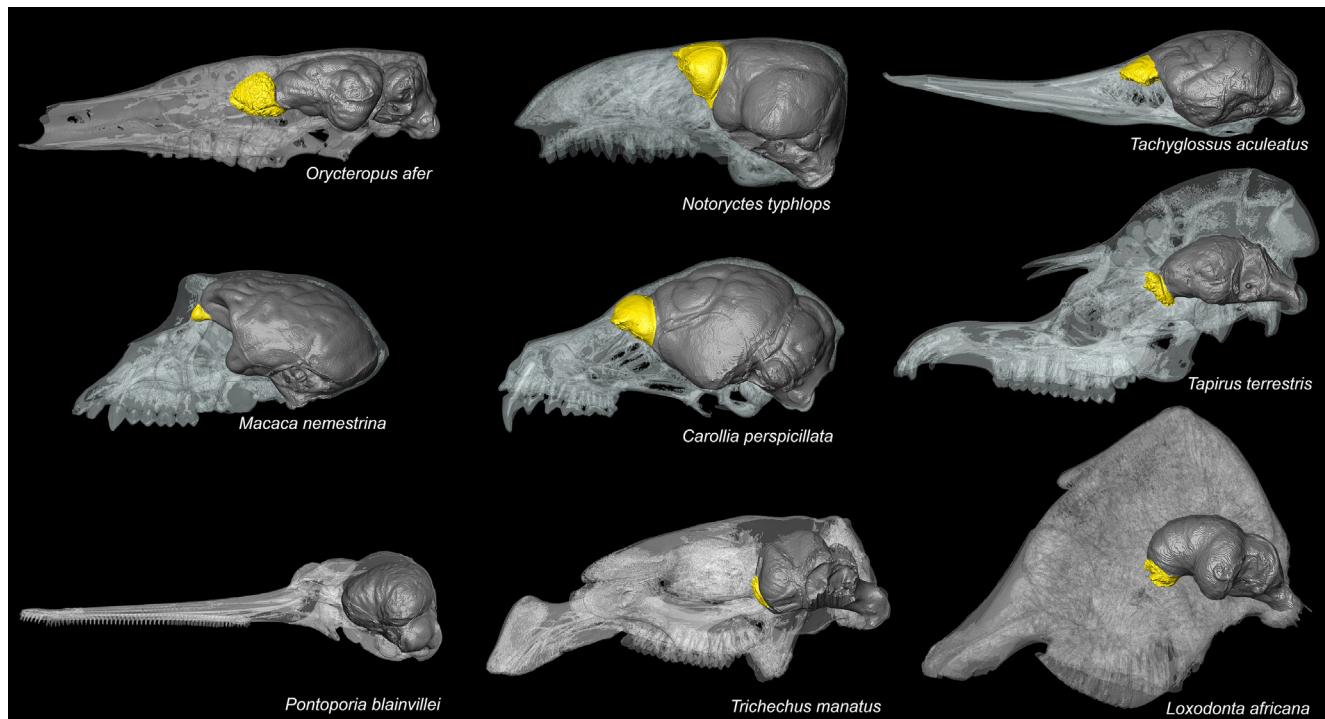
Fig. 4. Disparity of the olfactory bulb endocast across selected mammalian orders. The olfactory bulb endocast is shown in yellow, while the rest of the brain endocast is depicted in dark gray. Skulls are not shown to scale.

occipital condyle width to be a more precise metric in this case. Additionally, occipital condyle width was the variable closest to normality (Shapiro–Wilk P-value = 2.40E−02), and graphical verification confirmed that normality could be assumed. Therefore, we used this variable to scale the absolute volume of the olfactory bulb in a subsample dataset and in the full dataset, which comprises 71 species. The relative volume of the olfactory bulb endocast (now referred to as relatOB) is represented by the residuals from the LM of olfactory bulb volume against occipital condyle width.
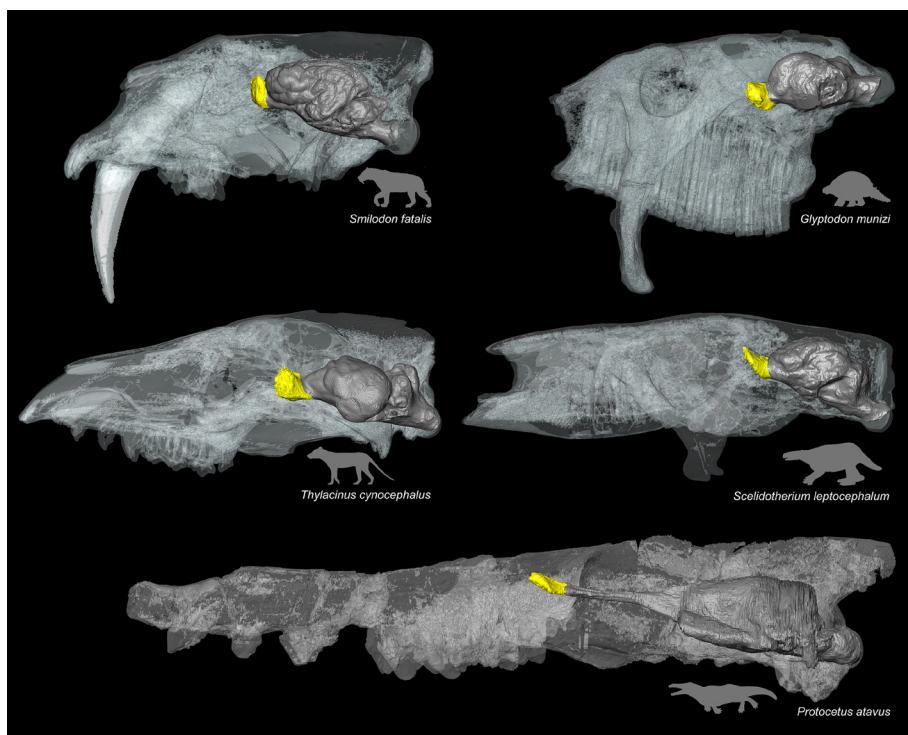
Fig. 5. Disparity of the olfactory bulb endocast across five emblematic extinct mammals. The olfactory bulb endocast is shown in yellow, while the rest of the brain endocast is depicted in dark gray. Skulls are not shown to scale. In compliance with PhyloPic guidelines, we credited T. Michael Keese, Ivan Iofrida, and Zimices (Julián Bayona) for the unmodified silhouettes of *Smilodon*, *Thylacinus*, and *Scelidotherium*, respectively, and provided the license links: https://creativecommons.org/licenses/by/3.0/ and https://creativecommons.org/licenses/by/4.0/. For illustrative purposes only, the broken canine of *Smilodon fatalis* LACM R37376 has been replaced with that of the specimen LACM 2001-3.

We then evaluated how different genomic variables explain relatOB. The genomic variables considered were OR (from 12, 54), VR, V1R, V2R, TAAR, TR, T1R, T2R (from 12), CombOR, and CombChemo. We tested the normality (Shapiro–Wilk) and heteroscedasticity (Breusch-Pagan) of the residuals of the nonlogged LM between relatOB and each genomic variable. Since the validity conditions were not met (with the exception of the case using OR from Han et al. (54)), we log10-transformed the genomic variables. We then retested normality (Shapiro–Wilk) and heteroscedasticity (Breusch-Pagan) of the residuals of the LM between relatOB and the log10-transformed genomic variables and recorded the AIC of the model. Since the validity conditions were met or nearly met in all cases, we performed correlation analyses using LM's test. Subsequently, we performed GLS without phylogeny and PGLS using four models: Martins with $\kappa = 0$, Martins with $\kappa = 1$, Grafen, and Brownian. We conducted AIC model comparisons for each of these models (Datasets S5 and S12). The results of the statistical tests are summarized in Table 1 and Datasets S11 and S18. We applied the same statistical approach to test for potential correlations between the absolute volume of the olfactory bulb (absOB) and the different genomic proxies (Datasets S3, S6, S14, and S17).

As suggested by several studies, olfaction in mysticetes, and more broadly in cetaceans, remains a field of active debate and ongoing investigation (45, 58–61). For this reason, we also performed all previously described analyses under various scenarios: *Eubalaena* excluded; *Pontoporia* excluded; both *Eubalaena* and *Pontoporia* excluded; and both *Eubalaena* and *Pontoporia* included. When the validity conditions were not met, we used Spearman's nonparametric correlation test. The impact of marsupials and monotremes on the recovered trends was tested in performing an additional set of analyses including only placental mammals and excluding *Eubalaena* and *Pontoporia* (Dataset S10).

Based on the dataset comprising all extant species of mammals, but excluding *Eubalaena* and *Pontoporia*, and using the most likely models, which in all cases were the LM, we first used the regression between absOB and occipital condyle width to calculate the residuals of the relatOB for three representatives of mammalian orders and five extinct species for which genomic data are not available. Using the regression between the residuals and the genomics values, we predicted CombChemo, CombOR, and OR according to the calculated residuals. The updated dataset, now including three representatives of mammalian orders for which genomic data are not available and/or five extinct species, was used to generate the figures (Figs. 1–3 and *SI Appendix*, Figs. S2 to S4). Since the predicted chemoreceptor gene counts were estimated from a dataset excluding cetaceans, an additional count prediction was performed for *Protocetus* using a dataset that included *Eubalaena*.

To display barplots of relatOB as well as CombChemo (Fig. 1 and *SI Appendix*, Figs. S2 to S4), we added 1 to the residuals from the LM between the absolute volume of the olfactory bulb and occipital condyle width. Both relatOB and CombChemo were then normalized, with their maximum values set to 1 for each variable.

All the analyses and plots were performed with R (62) and the following packages: APE (63), phytools (64), and ggplot2 (65).

2. Results and Discussion

2.1. The Functional Significance of the Olfactory Bulb Endocast.
Our study demonstrates a significant, positive correlation between relatOB and OR, CombOR, and CombChemo (Table 1 and Figs. 2 and 3*D*). Conversely, absOB is either weakly or not correlated with any of the genomic proxies tested (Fig. 3*F* and Datasets S3, S6, S14, and S17). From a neurobiological standpoint, absOB is hypothesized to reflect the number of olfactory neurons (66). Consequently, this absolute volume might serve as a potential proxy for olfactory capabilities in mammals, such as olfactory sensitivity and discrimination. However, when conducting comparative analyses across multiple groups with a broad range of body sizes, this proxy may primarily reflect species size rather than olfactory function (Fig. 3 *C* and *F*), as evidenced by our study encompassing all mammalian orders with body masses ranging from 10 grams to 23 tons. While absOB does exhibit a significant correlation with body size proxies (Fig. 3*C* and Datasets S4, S7, S12, and S15), the number of intact olfactory and chemosensory receptor genes appears independent of body mass (8, 11, 12, 17, 55, 67). Thus, at this taxonomic scale, absOB does not appear to be a robust proxy for studying olfaction in mammals.

The significant correlation between relatOB and OR, CombOR, and CombChemo (Table 1) is here assumed to mostly reflect the correlation between relatOB and the relative number of olfactory neurons. Its significant correlation with genomic proxies suggests that relatOB may serve as a robust proxy for studying olfaction in mammals. Martinez et al. (51) previously demonstrated that despite limitations in statistical power, in mammals, the number of intact OR genes might reflect mammalian species olfactory capabilities, such as sensitivity and discrimination. However, further work is needed to investigate the specific gene composition and its potential link with olfactory sensitivity. From a mechanistic perspective, high sensitivity is more likely to result from a large number of OR neurons expressing the same receptor type, along with strong convergence from receptor neurons to higher processing centers. Thus, relatOB may serve as an indirect measure of olfactory performance in mammals. However, this hypothesis requires further testing with a properly matched dataset that

Table 1. Results of correlation tests and associated statistics between the relative volume of the olfactory bulb and various genomic proxies of chemoreception for 61 mammalian species, excluding the cetaceans

Genomic variable	Correlation	LM r^2	LM s	LM P value	LM AIC	PGLS P value	Spearman corr	Spearman P value
OR	YES	0.58	1.32	6.14e−13	−11.85	6.14e−13	NA	NA
VR	WEAK	0.23	0.210	6.42E−05	25.48	5.25E−03	NA	NA
V1R	WEAK	0.22	0.220	7.06E−05	25.66	6.13E−03	NA	NA
V2R	WEAK	NA	NA	NA	NA	NA	0.34	6.80E−03
TAAR	WEAK	NA	NA	NA	NA	NA	0.26	0.05
TR	NO	NA	NA	NA	NA	NA	−0.25	0.06
T1R	NO	0.01	0.090	2.40E−01	40.70	0.03	NA	NA
T2R	WEAK	NA	NA	NA	NA	NA	−0.25	0.05
CombOR	YES	0.56	1.27	2.37E−12	−9.09	2.37E−12	NA	NA
CombChemo	YES	0.55	1.29	4.89E−12	−7.61	4.89E−12	NA	NA

OR: intact olfactory receptor genes; V1R and V2R: intact vomeronasal receptor genes types 1 and 2; TAAR: intact trace amine-associated receptors; T1R and T2R: intact taste receptor genes types 1 and 2. The total number of intact vomeronasal receptor (VR) genes was calculated by summing V1R and V2R. The total number of intact taste receptor (TR) genes was calculated by summing T1R and T2R. The total number of combined intact olfactory receptor (CombOR) genes was obtained by summing OR, V1R, V2R, and TAAR. The total number of combined intact chemoreceptor (CombChemo) genes was obtained by summing OR, V1R, V2R, TAAR, T1R, and T2R. s: slope (regression coefficient).

includes both relatOB and experimentally tested olfactory performance data.

Previous studies have examined the relationship between olfactory morphology and genomics using various proxies, such as the olfactory turbinals and the cribriform plate, yielding contrasting results. These discrepant results stem from differences in the genomic and morphological proxies selected as well as the taxonomic scale considered (10, 12, 17, 18, 23). Studies mostly based on primates have found a significant correlation between relatOB (based on actual brain volume, not brain endocast) and the number of intact OR genes (equivalent to the OR in this study), the sum of intact and truncated OR genes (excluding pseudogenized OR genes), as well as with the number of TAAR genes (9, 12). The relative volume of the olfactory bulbs in these studies were merged from multiple sources and initially obtained by Stephan et al. (68) and Pirlot and Kamiya (69). In these cases, the absolute volume of the olfactory bulb has been corrected for overall brain volume. For most species in these datasets, measurements focused exclusively on the main olfactory bulb, excluding the accessory olfactory bulb (68); however, in some species, the accessory olfactory bulb is included in these metrics (69), which may introduce inconsistencies in the methodology. Taken together with our dataset spanning all mammalian orders, these findings support the idea that, unlike olfactory turbinals, olfactory bulb comparative studies may be less affected by taxonomic scale, making it a more consistent and reliable proxy for studying mammalian olfaction.

Regarding the other olfactory and chemosensory receptor genes, we found weak significant correlations between relatOB and VR (Fig. 3E) as well as V1R, V2R, TAAR, and T2R (Table 1). However, we consider these correlations to be poor, as they are generally driven by a few species and associated with extremely low R^2 (Fig. 3E and Table 1). Likewise, no significant correlation was observed between relatOB and TR and T1R (Table 1). Models including combinations of genes (CombOR and CombChemo) instead of OR alone have significantly worse fits, suggesting that the correlation is primarily driven by the latter. These findings align with our expectations, as VR, V1R, V2R, TAAR, TR, T1R, and T2R represent a relatively small proportion of the overall chemoreceptor gene repertoire compared to OR. Also, VR, V1R, and V2R genes are predominantly associated with the vomeronasal organ, where sensory information is mainly processed in the accessory olfactory bulb. While isolating the accessory olfactory bulb using the actual brain (or diceCT images) is challenging but possible, it is impossible when considering mammal olfactory bulb endocasts. However, because the accessory olfactory bulb generally constitutes a small portion of the total olfactory bulb in most mammals, even substantial increases in its volume would have little effect on the overall olfactory bulb volume. In contrast, variations in the main olfactory bulb are directly reflected in changes in the total olfactory bulb volume. Therefore, a lack of correlation or a weak correlation between relatOB and the number of VR, V1R, and V2R genes is expected. In bats, species with an accessory olfactory bulb possess significantly more V1R genes than those without this subunit of the olfactory bulb (12). However, in some species with a reduced number of VR genes, the vomeronasal organ (likely associated with the accessory olfactory bulb) remains present (70). These overall interpretations are further supported by our model comparisons, which show that including combinations of genes (CombOR and CombChemo) instead of OR alone results in significantly worse fits (Table 1), suggesting that the correlation is primarily driven by OR.

All the scenarios tested to assess the robustness of the trends, i.e., the full dataset including all species; one species per mammalian order; *Eubalaena* excluded; *Pontoporia* excluded; both *Eubalaena* and *Pontoporia* excluded; entailed similar conclusions (Figs. 2 and 3 A and B and Table 1 and Datasets S3, S4–S9, and S11–S18). Only the correlations for chemoreceptor gene families that were weak or not significant varied across scenarios, further supporting the view that these weak correlations are not valid, as they are generally driven by a few outlying species.

Although relatOB may not provide as precise information as genomic proxies, it is still a valuable metric. From a genomic perspective, the metric is not perfect either, as it has been demonstrated that OR may be expressed outside the olfactory apparatus (71–73). For example, in the case of toothed whales (odontocetes) that present a drastic reduction of their OR genes (6, 12, 74) it is not possible to determine whether these few intact OR are involved in olfaction or are solely extranasal OR. Nevertheless, these extranasal OR likely represent a minor proportion of all expressed OR.

2.2. Olfaction and Species Ecology.

Studies have shown that ecological factors, such as habitat, along with diet, are reflected in variations in olfactory proxies that in turn likely relate to olfactory capabilities (7–9, 13–16, 20, 75). While a denser sampling is required to draw more refined conclusions, a clear ecological pattern already emerges from our data. The La Plata dolphin (*Pontoporia blainvillei*, Cetacea) shows the lowest CombChemo and lacks an identifiable olfactory bulb. While it remains unclear whether the few remaining intact OR genes serve olfactory functions or are extranasal OR expressed in other organs (73), this reduction in olfactory proxies strongly suggests reduced olfactory capabilities. Similar reductions in olfactory proxies have been observed in various aquatic or semiaquatic mammals (12, 13, 16). Notably, the right whale (*Eubalaena sp.*, Cetacea), the harbor seal (*Phoca vitulina*, Carnivora), the dugong (*Dugong dugon*, Sirenia), and the West Indian manatee (*Trichechus manatus*, Sirenia) also exhibits drastically reduced olfactory proxies, both genomically, with exceptionally low numbers of CombChemo, OR and VR genes (Figs. 2 and 3 A, D, and E and *SI Appendix,* Fig. S8), and anatomically, with a markedly reduced olfactory bulb. While a reduction of the olfactory organs is often associated with semi- or fully aquatic amniotes like cetaceans, the opposite phenomenon is also documented. Indeed, Burguera et al. (76) demonstrated that olfactory genes convergently expanded in nocturnal fishes capable of terrestrial exploration, which was accompanied by an increase in the relative number of olfactory bulb cells. This suggests that exposure to airborne odorants, or the lack thereof, can have an important impact on the evolution of the olfactory system.

Similarly, primates such as the common squirrel monkey (*Saimiri sciureus*), the Geoffroy's spider monkey (*Ateles geoffroyi*), the white-faced saki (*Pithecia pithecia*), and the southern pig-tailed macaque (*Macaca nemestrina*) show relatively reduced olfactory proxies both genomically and morphologically (*SI Appendix,* Fig. S8), aligning with known trends in primates which often show reduced olfactory proxies compared to other mammals (8).

At the other end of the spectrum, the African elephant (*Loxodonta africana*, Proboscidea) exhibits some of the highest olfactory proxies (Fig. 2 and *SI Appendix,* Figs. S2–S4), consistent with previous studies using genomic (8, 67) and morphological proxies (19, 23). The exceptionally high values observed in both olfactory proxies suggest strong selective pressures on olfaction, a likely substantial reliance on this sense, and potentially enhanced olfactory capabilities in this species (see also ref. 77).

Our results also highlight that the overall correlation between genomic and morphological proxies does not universally apply across all mammals. For instance, *Tachyglossus* ranks second in CombChemo but only 32nd in relatOB (*SI Appendix,* Figs. S9 and S10). Such discrepancies offer promising models for further

investigation into the mechanisms of odor detection and their interplay with olfactory proxies. It is possible that specific gene families drive OR expansion to enhance sensitivity to certain odor types, while morphological or developmental constraints may limit relatOB, potentially compensated by increased neuronal density.

For the three mammalian orders lacking genomic data, the relatOB of the gray-bellied caenolestid (*Caenolestes caniventer*, Paucituberculata) falls within the range of *Canis*, while the relatOB of the northern brown bandicoot (*Isoodon macrourus*, Peramelemorphia) and the southern marsupial mole (*Notoryctes typhlops*, Notoryctemorphia) falls among the mammals with the largest relatOB, comparable to *Erinaceus* (Fig. 2 and *SI Appendix,* Fig. S4). For *Caenolestes* and *Isoodon*, these results may be linked to their relatively specialized diet, which consists of earthworms and arthropods from leaf litter (78). This diet has been observed in other mammals with elongated snouts and specialized feeding habits, which are often (e.g., in the case of earthworm diet specialization; 15) but not always (21) associated with enhanced olfactory proxies. For *Notoryctes*, the prevailing hypothesis suggests that subterranean species may rely more heavily on olfactory cues due to their reduced vision (79).

2.3. Estimating OR Genes in Extinct Mammals.

Based on the previously established relationship between OR and olfactory capabilities in mammals (51), estimating OR in species lacking genomic data—such as extinct taxa—may provide a reliable indirect proxy for assessing their olfactory capabilities. The saber-toothed cat (*Smilodon fatalis*) shows a reduced relatOB compared to the extant *Canis lupus* (Canidae), with a value that falls within the range of *Artibeus*, *Lama*, and *Mus* (Fig. 2). Our estimate of OR (715 OR, Fig. 3D) aligns with the previous estimate based on the cribriform plate (521 to 685 OR; 23). The ground sloth (*Scelidotherium leptocephalum*) also has a reduced relatOB (Fig. 2) compared to extant species such as the southern tamandua (*Tamandua tetradactyla*, Pilosa), and the giant anteater (*Myrmecophaga tridactyla*, Pilosa). The glyptodon (*Glyptodon munizi*) shows a drastic reduction in relatOB compared to extant species such as the nine-banded armadillo (*Dasypus novemcinctus*, Cingulata) and the southern three-banded armadillo (*Tolypeutes matacus*, Cingulata), falling within the range of mammals with the lowest relatOB (Fig. 2). While the anatomy of glyptodont nasal cavity still has to be studied in details, it is noteworthy that the maxilloturbinal—implicated in heat and moisture conservation as well as in the protection of the lower respiratory tract and the olfactory apparatus—is particularly developed (80). Since it has been demonstrated that, in small mammals, a trade-off exists between the maxilloturbinal (along with the nasoturbinal) and the olfactory turbinals (16, 81), such selective pressures may have constrained the olfactory system of *Glyptodon*. The relatOB of the protocetid whale (*Protocetus atavus*) falls within the range of mammals with a reduced olfactory apparatus; however, it is significantly larger than that of the extant cetaceans, sirenians, and primates sampled in this study. This suggests that the olfactory apparatus of this middle Eocene protocetid may not have been yet under strong selective pressure (or relaxed selective pressure) for reduction, as is typically associated with early cetacean evolution (48). Finally, the relatOB of the Tasmanian tiger (*Thylacinus cynocephalus*, Marsupialia) ranks among the species with relatively high values (Figs. 2 and 5 and *SI Appendix,* Fig. S4), similar to the other sampled Dasyuromorphians, such as the Tasmanian devil (*Sarcophilus harrisii*) and the numbat (*Myrmecobius fasciatus*; Figs. 2 and *SI Appendix,* Fig. S4). However, the Tasmanian tiger shows a strong discrepancy between its morphology and

genomic data when considering the OR from the CORD (661 OR; 54), compared to our estimation based on relatOB (1252 OR, Fig. 3D and *SI Appendix,* Fig. S1). Upon investigation, the Tasmanian tiger genome ranks 15th lowest in BUSCO score among the 64 genomes examined (Dataset S1), yet still shows a relatively high score of 89%. Similarly, *Sarcophilus harrisii* and *Myrmecobius fasciatus* exhibit larger relatOB than expected based on their genomic data (Figs. 2 and 3D). These mismatches indicate the need for further investigation into certain marsupial groups (82–85). However, deviations from the regression line are not restricted to marsupials (Fig. 2), and the estimated 1252 intact OR genes for the Tasmanian tiger, derived from this regression, may not fully capture this variation. We hence suggest to directly use the relative size of the OB rather than attempting to estimate the number of OR genes, which can be subject to various biases involving suboptimal genome quality or imperfect correlation with morphological traits.

2.4. Conclusion.

While our results support a functional link between genomic and morphological proxies, the exact nature of how relatOB and OR affects olfactory capabilities, such as sensitivity, discrimination, or both, remains insufficiently understood. It is likely that a given relatOB or OR count may correspond to different olfactory capabilities, in response to ecological constraints, olfactory neuron density, and gene composition. Further studies are needed to better understand the mechanisms of odorant detection in relation to olfactory performance. Our findings provide a basis for these future investigations and advance our understanding of the selective pressures that have shaped mammalian olfaction.

With the increasing availability of high-quality genomes, particularly for orders currently represented by only a single genome, it will become possible to refine analyses and interpretations. A more phylogenetically balanced dataset, comprising multiple species per order, will allow for more precise correlations and the development of group-specific regression models within certain clades.

Overall, we demonstrated that the relative volume of the olfactory bulb endocast reflects the number of intact OR genes and the total number of intact chemoreceptor genes, highlighting its functional significance. We therefore suggest that the relative volume of the olfactory bulb endocast is a reliable proxy for studying mammalian olfaction, providing an important avenue for exploring the evolution of this sense in species for whom performance and genomic data are not available, including extinct ones.

Author affiliations: ªStaatliches Museum für Naturkunde, Stuttgart DE-70191, Germany; ᵇDepartment of Algal Development and Evolution, Max Planck Institute for Biology, Tübingen 72076, Germany; ᶜDepartment of Paleontology, University of Zurich, Zurich, Switzerland; ᵈNaturhistorisches Museum der Burgergemeinde, Bern, Switzerland; ᵉInstitute of Ecology and Evolution, Universität Bern, Bern, Switzerland; ᶠScience Departments, The Natural History Museum, London, United Kingdom; ᵍCentre de Recherche en Paléontologie—Paris (CR2P, UMR 7207), Sorbonne Université, Muséum National d'Histoire Naturelle, CNRS, Paris F-75005, France; ʰEuropean Synchrotron Radiation Facility, Grenoble 38000, France; ⁱSenckenberg Centre for Human Evolution and Palaeoenvironment at the Eberhard Karls University of Tübingen, Tübingen 72074, Germany; ʲDepartment of Geosciences, Faculty of Sciences, Eberhard Karls University of Tübingen, Tübingen 72074, Germany; ᵏInstitute for Photon Science and Synchrotron Radiation (IPS), Karlsruhe Institute of Technology (KIT), Eggenstein-Leopoldshafen 76344, Germany; ˡLaboratory for Applications of Synchrotron Radiation (LAS), Karlsruhe Institute of Technology (KIT), Karlsruhe 76131, Germany; and ᵐInstitut des Sciences de l'Evolution de Montpellier, Univ. Montpellier, CNRS, Institut de recherche pour le développement (IRD), Montpellier Cedex 05 34095, France

1. L. Buck, R. Axel, A novel multigene family may encode odorant receptors: A molecular basis for odor recognition. *Cell* **65**, 175–187 (1991).
2. K. Lindblad-Toh *et al.*, Genome sequence, comparative analysis and haplotype structure of the domestic dog. *Nature* **438**, 803–819 (2005).
3. M. Zarzo, The sense of smell: Molecular basis of odorant recognition. *Biol. Rev.* **82**, 455–479 (2007).
4. Y. Niimura, M. Nei, Extensive gains and losses of olfactory receptor genes in mammalian evolution. *PLoS One* **2**, e708 (2007).
5. S. Hayden *et al.*, Ecological adaptation determines functional mammalian olfactory subgenomes. *Genome Res.* **20**, 1–9 (2010).
6. T. Kishida, S. Kubota, Y. Shirayama, H. Fukami, The olfactory receptor gene repertoires in secondary-adapted marine vertebrates: Evidence for reduction of the functional proportions in cetaceans. *Biol. Lett.* **3**, 428–430 (2007).
7. S. Hayden, E. C. Teeling, The molecular biology of vertebrate olfaction. *Anat. Rec.* **297**, 2216–2226 (2014).
8. G. M. Hughes *et al.*, The birth and death of olfactory receptor gene families in mammalian niche adaptation. *Mol. Biol. Evol.* **35**, 1390–1406 (2018).
9. Y. Niimura, A. Matsui, K. Touhara, Acceleration of olfactory receptor gene loss in primate evolution: Possible link to anatomical change in sensory systems and dietary transition. *Mol. Biol. Evol.* **35**, 1437–1450 (2018).
10. M. J. Christmas *et al.*, Evolutionary constraint and innovation across hundreds of placental mammals. *Science* **380**, eabn3943 (2023).
11. M. Courcelle, P.-H. Fabre, E. J. P. Douzery, Phylogeny, ecology, and gene families covariation shaped the olfactory subgenome of rodents. *Genome Biol. Evol.* **15**, evad197 (2023).
12. M. Policarpo, M. W. Baldwin, D. Casane, W. Salzburger, Diversity and evolution of the vertebrate chemoreceptor gene repertoire. *Nat. Commun.* **15**, 1421 (2024).
13. B. Van Valkenburgh *et al.*, Aquatic adaptations in the nose of carnivorans: Evidence from the turbinates. *J. Anat.* **218**, 298–310 (2011).
14. P. A. Green *et al.*, Respiratory and olfactory turbinal size in canid and arctoid carnivorans. *J. Anat.* **221**, 609–621 (2012).
15. Q. Martinez *et al.*, Convergent evolution of an extreme dietary specialisation, the olfactory system of worm-eating rodents. *Sci. Rep.* **8**, 17806 (2018).
16. Q. Martinez *et al.*, Convergent evolution of olfactory and thermoregulatory capacities in small amphibious mammals. *Proc. Natl. Acad. Sci.* **117**, 8958–8965 (2020).
17. Q. Martinez, M. Courcelle, E. Douzery, P.-H. Fabre, When morphology does not fit the genomes: The case of rodent olfaction. *Biol. Lett.* **19**, 20230080 (2023).
18. Q. Martinez *et al.*, Turbinal bones are still one of the last frontiers of the tetrapod skull: Hypotheses, challenges and perspectives. *Biol. Rev.* **99**, 2304–2337 (2024).
19. Q. Martinez *et al.*, Turbinal bones disparity across placental mammals. *Anat. Rec.*, 10.1002/ar.25552 (2024).
20. A. D. Melin *et al.*, Anatomy and dietary specialization influence sensory behaviour among sympatric primates. *Proc. R. Soc. B Biol. Sci.* **289**, 20220847 (2022).
21. M. Wright *et al.*, Sniffing out morphological convergence in the turbinal complex of myrmecophagous placentals. *Anat. Rec.*, 10.1002/ar.25603 (2024).
22. D. J. Bird, A. Amirkhanian, B. Pang, B. Van Valkenburgh, Quantifying the cribriform plate: Influences of allometry, function, and phylogeny in Carnivora. *Anat. Rec.* **297**, 2080–2092 (2014).
23. D. J. Bird *et al.*, Olfaction written in bone: Cribriform plate size parallels olfactory receptor gene repertoires in mammalia. *Proc. R. Soc. B Biol. Sci.* **285**, 20180100 (2018).
24. D. J. Bird, C. Jacquemetton, S. A. Buelow, A. W. Evans, B. Van Valkenburgh, Domesticating olfaction: Dog breeds, including scent hounds, have reduced cribriform plate morphology relative to wolves. *Anat. Rec.* **304**, 139–153 (2021).
25. I. Ruf, W. Maier, P. G. Rodrigues, C. L. Schultz, Nasal anatomy of the non-mammaliaform cynodont *Brasilitherium riograndensis* (Eucynodontia, Therapsida) reveals new insight into mammalian evolution. *Anat. Rec.* **297**, 2018–2030 (2014).
26. I. K. Lundeen, E. C. Kirk, Internal nasal morphology of the Eocene primate *Rooneyia viejaensis* and extant Euarchonta: Using μct scan data to understand and infer patterns of nasal fossa evolution in primates. *J. Hum. Evol.* **132**, 137–173 (2019).
27. E. Peri, P. D. Gingerich, G. Aringhieri, G. Bianucci, Reduction of olfactory and respiratory turbinates in the transition of whales from land to sea: The semiaquatic middle Eocene *Aegyptocetus tarfa*. *J. Anat.* **236**, 98–104 (2020).
28. T. B. Rowe, T. E. Macrini, Z.-X. Luo, Fossil evidence on origin of the mammalian brain. *Science* **332**, 955–957 (2011).
29. V. Weisbecker *et al.*, Global elongation and high shape flexibility as an evolutionary hypothesis of accommodating mammalian brains into skulls. *Evolution* **75**, 625–640 (2021).
30. O. C. Bertrand *et al.*, Brawn before brains in placental mammals after the end-Cretaceous extinction. *Science* **376**, 80–85 (2022).
31. J. Benoit *et al.*, "Paleoneurology of the Proboscidea (Mammalia, Afrotheria): Insights from Their Brain Endocast and Labyrinth" in *Paleoneurology of Amniotes*, M. T. Dozo, A. Paulina-Carabajal, T. E. Macrini, S. Walsh, Eds. (Springer International Publishing, 2023), pp. 579–644.
32. O. C. Bertrand, M. T. Silcox, "Brain evolution in fossil rodents: A starting point" in *Paleoneurology of Amniotes: New Directions in the Study of Fossil Endocasts*, M. T. Dozo, A. Paulina-Carabajal, T. E. Macrini, S. Walsh, Eds. (Springer International Publishing, 2023), pp. 645–680.
33. G. A. Lyras, A. A. E. van der Geer, L. Werdelin, "Paleoneurology of carnivora" in *Paleoneurology of Amniotes: New Directions in the Study of Fossil Endocasts*, M. T. Dozo, A. Paulina-Carabajal, T. E. Macrini, S. Walsh, Eds. (Springer International Publishing, 2023), pp. 681–710.
34. T. E. Macrini, J. Orihuela, "Evolution of the brain and sensory structures in sirenia" in *Paleoneurology of Amniotes: New Directions in the Study of Fossil Endocasts*, M. T. Dozo, A. Paulina-Carabajal, T. E. Macrini, S. Walsh, Eds. (Springer International Publishing, 2023), pp. 557–577.
35. M. J. Orliac, J. Maugoust, A. Balcarcel, E. Gilissen, "Paleoneurology of artiodactyla, an overview of the evolution of the artiodactyl brain" in *Paleoneurology of Amniotes: New Directions in the Study of Fossil Endocasts*, M. T. Dozo, A. Paulina-Carabajal, T. E. Macrini, S. Walsh, Eds. (Springer International Publishing, 2023), pp. 507–555.
36. T. B. Rowe, "Evolution of the mammalian neurosensory system: Fossil evidence and major events" in *Paleoneurology of Amniotes: New Directions in the Study of Fossil Endocasts*, M. T. Dozo, A. Paulina-Carabajal, T. E. Macrini, S. Walsh, Eds. (Springer International Publishing, 2023), pp. 365–422.
37. M. M. Lang *et al.*, But how does it smell? An investigation of olfactory bulb size among living and fossil primates and other euarchontoglirans. *Anat. Rec.*, 10.1002/ar.25651 (2025).
38. E. Mollo *et al.*, Taste and smell: A unifying chemosensory theory. *Q. Rev. Biol.* **97**, 69–94 (2022).
39. D. Boyer, G. Gunnell, S. Kaufman, T. McGeary, Morphosource: Archiving and sharing 3-d digital specimen data. *Paleontol. Soc. Pap.* **22**, 157–181 (2016).
40. P. D. Lösel *et al.*, Introducing Biomedisa as an open-source online platform for biomedical image segmentation. *Nat. Commun.* **11**, 5577 (2020).
41. O. C. Bertrand, M. T. Silcox, First virtual endocasts of a fossil rodent: <i>Ischyromys typus</i> (Ischyromyidae, Oligocene) and brain evolution in rodents. *J. Vertebr. Paleontol.* **36**, e1095762 (2016).
42. J. Orihuela, L. W. Viñola López, T. E. Macrini, First cranial endocasts of early Miocene sirenians (Dugongidae) from the West Indies. *J. Vertebr. Paleontol.* **39**, e1584565 (2019).
43. J. Shoshani, W. J. Kupsky, G. H. Marchant, Elephant brain: Part I: Gross morphology, functions, comparative anatomy, and evolution. *Brain Res. Bull.* **70**, 124–157 (2006).
44. J. Benoit, N. Crumpton, S. Mérigeaud, R. Tabuce, A memory already like an elephant's? The advanced brain morphology of the last common ancestor of Afrotheria (Mammalia). *Brain. Behav. Evol.* **81**, 154–169 (2013).
45. D. A. Waugh, J. G. M. Thewissen, The pattern of brain-size change in the early evolution of cetaceans. *PLoS One* **16**, e0257803 (2021).
46. R. K. Engelman, Occipital condyle width (OCW) is a highly accurate predictor of body mass in therian mammals. *BMC Biol.* **20**, 54 (2022).
47. N. S. Upham, J. A. Esselstyn, W. Jetz, Inferring the mammal tree: Species-level sets of phylogenies for questions in ecology, evolution, and conservation. *PLoS Biol.* **17**, e3000494 (2019).
48. E. Berger *et al.*, The endocranial anatomy of protocetids and its implications for early whale evolution. *Evolution* **79**, 2306–2314 (2025), 10.1093/evolut/qpaf109.
49. F. A. Smith *et al.*, Body mass of late Quaternary mammals. *Ecology* **84**, 3403–3403 (2003).
50. H. Stephan, Methodische Studien über den quantitativen Vergleich architektonischer Struktureinheiten des Gehirns. *Z Wiss Zool.* **164**, 143–172 (1960).
51. Q. Martinez, E. Amson, M. Laska, Does the number of functional olfactory receptor genes predict olfactory sensitivity and discrimination performance in mammals? *J. Evol. Biol.* **37**, 238–247 (2024).
52. L. R. Yohe, M. Fabbri, M. Hanson, B.-A.S. Bhullar, Olfactory receptor gene evolution is unusually rapid across Tetrapoda and outpaces chemosensory phenotypic change. *Curr. Zool.* **66**, 505–514 (2020).
53. T. Kishida *et al.*, Loss of olfaction in sea snakes provides new perspectives on the aquatic adaptation of amniotes. *Proc. R. Soc. B Biol. Sci.* **286**, 20191828 (2019).
54. W. Han, Y. Wu, L. Zeng, S. Zhao, Building the Chordata olfactory receptor database using more than 400, 000 receptors annotated by Genome2OR. *Sci. China Life Sci.* **65**, 2539–2551 (2022), 10.1007/s11427-021-2081-6.
55. Y. Niimura *et al.*, Synchronized expansion and contraction of olfactory, vomeronasal, and taste receptor gene families in hystricomorph rodents. *Mol. Biol. Evol.* **41**, msae071 (2024).
56. Y. Niimura, On the origin and evolution of vertebrate olfactory receptor genes: Comparative genome analysis among 23 chordate species. *Genome Biol. Evol.* **1**, 34–44 (2009).
57. S. D. Liberles, L. B. Buck, A second class of chemosensory receptors in the olfactory epithelium. *Nature* **442**, 645–650 (2006).
58. J. G. M. Thewissen, J. George, C. Rosa, T. Kishida, Olfaction and brain size in the bowhead whale (*Balaena mysticetus*). *Mar. Mammal Sci.* **27**, 282–294 (2011).
59. T. Kishida, "Evolution of the mammalian brain with a focus on the whale olfactory bulb|SpringerLink" in *Brain Evolution by Design: From Neural Origin to Cognitive Architecture*, (Springer Japan, 2017), pp. 329–342.
60. I. C. Farnkopf *et al.*, Olfactory epithelium and ontogeny of the nasal chambers in the bowhead whale (*Balaena mysticetus*). *Anat. Rec.* **305**, 643–667 (2022).
61. A. Hirose *et al.*, Localized expression of the olfactory receptor genes in the olfactory organ of common minke whales. *Int. J. Mol. Sci.* **25**, 3855 (2024).
62. R Core Team, *R: A language and environment for statistical computing. R Foundation for Statistical Computing*. Vienna Austria URL Httpswww R-Proj. Org (2025).
63. E. Paradis, J. Claude, K. Strimmer, APE: Analyses of phylogenetics and evolution in R language. *Bioinformatics* **20**, 289–290 (2004).
64. L. J. Revell, Phytools: An R package for phylogenetic comparative biology (and other things). *Methods Ecol. Evol.* **3**, 217–223 (2012).
65. H. Wickham, ggplot2: Elegant Graphics for Data Analysis. (Springer-Verl, N. Y., 2016).
66. S. Aicardi *et al.*, The olfactory system of sharks and rays in numbers. *Anat. Rec.*, 10.1002/ar.25537 (2024).
67. Y. Niimura, A. Matsui, K. Touhara, Extreme expansion of the olfactory receptor gene repertoire in African elephants and evolutionary dynamics of orthologous gene groups in 13 placental mammals. *Genome Res.* **24**, 1485–1496 (2014).
68. H. Stephan, H. Frahm, G. Baron, New and revised data on volumes of brain structures in insectivores and primates (1981), 10.1159/000155963.
69. P. Pirlot, T. Kamiya, Relative size of brain and brain components in three gliding placentals (Dermoptera: Rodentia). *Can. J. Zool.* **60**, 565–572 (1982).

70. L. R. Yohe, N. T. Krell, An updated synthesis of and outstanding questions in the olfactory and vomeronasal systems in bats: Genetics asks questions only anatomy can answer. *Anat. Rec.* **306**, 2765–2780 (2023).

71. S. Wojcik *et al.*, Functional characterization of the extranasal OR2A4/7 expressed in human melanocytes. *Exp. Dermatol.* **27**, 1216–1223 (2018).

72. S. Kalra *et al.*, Challenges and possible solutions for decoding extranasal olfactory receptors. *FEBS J.* **288**, 4230–4241 (2021).

73. M. R. Beito, S. Ashraf, D. Odogwu, R. Harmancey, Role of ectopic olfactory receptors in the regulation of the cardiovascular–kidney–metabolic axis. *Life* **14**, 548 (2024).

74. T. Kishida, J. Thewissen, T. Hayakawa, H. Imai, K. Agata, Aquatic adaptation and the evolution of smell and taste in whales. *Zool. Lett.* **1**, 9 (2015).

75. L. R. Yohe *et al.*, Ecological constraints on highly evolvable olfactory receptor genes and morphology in neotropical bats. *Evolution* **76**, 2347–2360 (2022).

76. D. Burguera *et al.*, Expanded olfactory system in ray-finned fishes capable of terrestrial exploration. *BMC Biol.* **21**, 163 (2023).

77. A. Rizvanovic, M. Amundin, M. Laska, Olfactory discrimination ability of Asian elephants (*Elephas maximus*) for structurally related odorants. *Chem. Senses* **38**, 107–118 (2013).

78. R. A. Mittermeier, D. E. Wilson, *Handbook of the Mammals of the World–Volume 5: Monotremes and Marsupials* (2015), ed. Lynxs.

79. R. Partha *et al.*, Subterranean mammals show convergent regression in ocular genes and enhancers, along with adaptation to tunneling. *eLife* **6**, e25884 (2017).

80. J. Fernicola, N. Toledo, M. Bargo, S. Vizcaíno, A neomorphic ossification of the nasal cartilages and the structure of paranasal sinus system of the glyptodontNeosclerocalyptus Paula Couto 1957 (Mammalia, Xenarthra). *Palaeontol. Electron.* **15**, 27 (2012).

81. Q. Martinez *et al.*, Mammalian maxilloturbinal evolution does not reflect thermal biology. *Nat. Commun.* **14**, 4425 (2023).

82. V. Weisbecker, A. Goswami, Brain size, life history, and metabolism at the marsupial/placental dichotomy. *Proc. Natl. Acad. Sci.* **107**, 16216–16221 (2010).

83. V. Weisbecker, K. Ashwell, D. Fisher, An improved body mass dataset for the study of marsupial brain size evolution. *Brain. Behav. Evol.* **82**, 81–82 (2013).

84. V. Weisbecker, S. Blomberg, A. W. Goldizen, M. Brown, D. Fisher, The evolution of relative brain size in marsupials is energetically constrained but not driven by behavioral complexity. *Brain. Behav. Evol.* **85**, 125–135 (2015).

85. T. E. Macrini, M. Leary, V. Weisbecker, "Evolution of the brain and sensory structures in metatherians" in *Paleoneurology of Amniotes: New Directions in the Study of Fossil Endocasts*, M. T. Dozo, A. Paulina-Carabajal, T. E. Macrini, S. Walsh, Eds. (Springer International Publishing, 2023), pp. 423–456.

86. Q. Martinez *et al.*, The olfactory bulb endocast as a proxy for mammalian olfaction. MorphoSource. https://www.morphosource.org/projects/000791369. Deposited 1 November 2025.